

Note: This is a draft of a paper submitted for publication. Contents of this paper should not be quoted or referred to without permission of the author(s).

Submitted at the *Fall 2000 Materials Research Society Meeting*
Symposium Proceedings, "Microstructural Processes in Irradiated Materials"

Ion-Irradiation-Induced Amorphization of Cadmium Niobate Pyrochlore

A. Meldrum,¹ K. Beaty,¹ L. A. Boatner,² and C. W. White².

¹Department of Physics, University of Alberta, Edmonton, AB T6G Canada

²Solid State Division, Oak Ridge National Laboratory, Oak Ridge, TN 37831

The submitted manuscript has been authored by a contractor of the U.S. Government under contract No. DE-AC05-00OR22725. Accordingly, the U.S. Government retains a nonexclusive, royalty-free license to publish or reproduce the published form of this contribution, or allow others to do so, for U.S. Government purposes."

Prepared by the
SOLID STATE DIVISION
OAK RIDGE NATIONAL LABORATORY
Managed by
UT-BATTELLE, LLC, for the
U.S. DEPARTMENT OF ENERGY
Under Contract No. DE-AC05-00OR22725

ION-IRRADIATION-INDUCED AMORPHIZATION OF CADMIUM NIOBATE PYROCHLORE

A. Meldrum and K. Beaty, Dept. of Physics, University of Alberta, Edmonton AB, T5N 2A3, Canada

L. A. Boatner and C. W. White, Solid State Division, Oak Ridge National Laboratory, Oak Ridge TN 37831 USA

Introduction

Pyrochlores represent a large class of compounds with the general chemical formula $A_2B_2O_7$. The pyrochlore structure consists of interconnected AO_8 and BO_6 cation polyhedra [1] where the BO_6 octahedra are slightly distorted and form a continuous corner-sharing network. The large, 8-fold coordinated A-site cations and the seventh oxygen occupy channels in the $(B_2O_6)_\infty$ network of octahedra [1,2]. The structure is an anion-deficient MX_2 fluorite structure in which the A and B cations are ordered on the M sites. One eighth of the X anions are absent in the pyrochlore structure, and the resulting oxygen vacancies are ordered on the anion sublattice [2].

Recent *in-situ* ion irradiation experiments have focused on the effects of chemical composition and incident ion mass and energy on the irradiation-induced amorphization of several pyrochlore compositions. $Gd_2Ti_2O_7$ has been the subject of considerable study since it is one of the three main actinide-bearing phases of SYNROC, – a polyphase ceramic waste form proposed for the disposition of high-level nuclear waste. Replacement of the Gd with other lanthanide elements or Ca has been found to have a relatively minor effect on the kinetics of irradiation-induced amorphization; however, the substitution of Ti with Zr in increasing concentrations sharply increases the resistance to amorphization even at cryogenic temperatures [3]. Pyrochlore containing a variety of A-site cations, including mixtures of Ca, U, [4,5] and various lanthanides [6] are easily amorphized at room temperature, and in fact, amorphization can be induced at temperatures as high as 1030 K.

The previous studies of radiation damage effects in pyrochlores have employed either impure natural crystals with relatively uncertain geological histories or polycrystalline synthetic, pressed and sintered pellets. All previous ion-beam investigations have used pyrochlores of the +3,+4 cation valence group. In the present work, we investigate the effects of ion irradiation using relatively large (up to 15 x 15 x 5 mm) high-purity synthetic single crystals of the cadmium/niobium +2,+5 pyrochlore, $Cd_2Nb_2O_7$.

Experimental

Crystals of $Cd_2Nb_2O_7$ were grown by means of a high-temperature solvent (flux) technique. The resulting single crystals were prepared for the *in-situ* ion-irradiation/TEM analysis experiments by hand polishing to a thickness of approximately 10 μm and subsequent ion milling to perforation at room temperature using 4 keV Ar^+ ions at an incident angle of 20°. These specimens were then irradiated *in-situ* in an electron microscope at the HVEM-Tandem Facility at Argonne National Laboratory [7]. The irradiations were carried out with either 1200 keV Xe^{2+} or 280 keV Ne^+ ions at

temperatures from 20 to 1100 K. The ion flux was $1.7 \times 10^{12} \text{ cm}^{-2}\text{s}^{-1}$. The electron microscope was operated at 300 kV, and the electron beam was not incident on the specimen for most of the ion-irradiation time. Selected-area electron diffraction was used to determine the dose necessary to amorphize the specimen. The experiments were continued until the electron-diffraction maxima disappeared, as determined by visual examination of the phosphor screen, and the electron-diffraction pattern consisted only of the diffuse halo characteristic of an amorphous material. The thickness of the specimens was estimated to be $\sim 100 \text{ nm}$ by using combined thickness-fringe and convergent-beam electron-diffraction measurements. The room-temperature experiments were repeated three times in order to estimate the mean deviation. This was converted to a percentage of the average value, and the same percentage was used to calculate error bars on all the data points.

The $\text{Cd}_2\text{Nb}_2\text{O}_7$ crystals that also exhibited high-quality growth faces were selected for use in the combined ion implantation and RBS analysis experiments. The most highly developed growth faces corresponded to $\{111\}$ family of crystallographic planes, and these were used for most of the experiments. The specimens were mounted by spring-clipping onto a steel backing plate for ion implantation. One half of each sample was masked and was not implanted. The beam current was less than $0.5 \mu\text{A}/\text{cm}^2$ so thermally conductive paint was not applied. The duration of the implant was from seconds to a few minutes. All of the implantations were carried out at room temperature. The samples were tilted 7° away from the incident ion beam to minimize channeling effects. Specimens were irradiated with either 320 keV Xe^{2+} to fluences ranging from 5×10^{12} to 1×10^{15} ions/ cm^2 , or with 70 keV Ne^+ to fluences from 3×10^{14} to 1×10^{16} ions/ cm^2 . At these energies, both ion types have a projected range of approximately 60 nm. The specimens were implanted to a low ion fluence and were then removed from the implanter, and Rutherford Backscattering analysis (RBS) in the channeling mode was performed using a 2.3 MeV He^+ ion beam with the detector at an angle of 160° relative to the incident He^+ beam. Each specimen was initially aligned in the usual manner by finding the minimum yield in the unimplanted (masked) portion of the crystal. The specimen was then linearly translated so that the He beam impinged on the implanted region of the crystal, and a new spectrum was obtained. Random yields were obtained by tilting the unirradiated part of the crystal away from the zone axis and then rotating over an angle of $\pm 5^\circ$ during data collection. The specimens were subsequently returned to the ion implanter for the accumulation of an additional ion dose, and the process was repeated until the channeling yield from the near-surface region matched the random yield.

Results and Discussion

In-situ experiments

$\text{Cd}_2\text{Nb}_2\text{O}_7$ was amorphized at room temperature by both the Ne^+ and Xe^{2+} irradiations. At low fluences (*i.e.*, less than one third of the total fluence for amorphization), the $\{022\}$ diffraction maxima from the pyrochlore lattice gradually disappeared, but the $\{044\}$ maxima remained intense (Fig. 1). With increasing dose, the $\{044\}$ diffraction spots gradually decreased in intensity, and concurrently, a diffraction halo characteristic of an

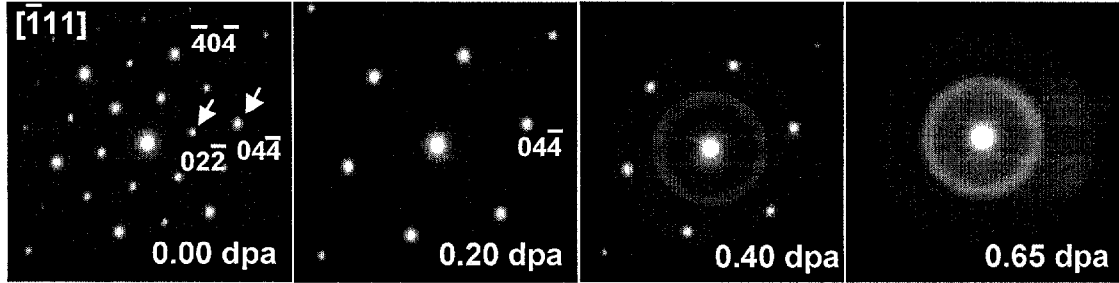


Fig. 1. Electron-diffraction patterns for $\text{Cd}_2\text{Nb}_2\text{O}_7$ irradiated with 280 keV Ne^+ . The dose is given in the bottom right corner of each diffraction pattern.

amorphous phase increased in intensity. The electron-diffraction patterns presented in Figure 1 for the case of Ne^+ irradiation show that, in fact, $\text{Cd}_2\text{Nb}_2\text{O}_7$ does not become amorphous directly, but rather that it transforms to the disordered defect-fluorite structure at intermediate ion doses. Disordering prior to amorphization has been observed in several other pyrochlore compositions [4-6]. The ion fluence required for the amorphization of $\text{Cd}_2\text{Nb}_2\text{O}_7$, as measured by electron diffraction, is given in Table 1. These values were converted to an amorphization dose (D_c) in dpa, using SRIM to determine the number of displacements per ion over the thickness of the specimen (the displacement energy was assumed to be 25 eV to be consistent with previous studies). The temperature dependence of the amorphization dose for the Ne^+ and Xe^{2+} ion irradiation of $\text{Cd}_2\text{Nb}_2\text{O}_7$ is plotted in Fig. 2. For Ne^+ irradiation, the amorphization dose is relatively constant at ~ 0.3 dpa at temperatures below ~ 150 K, compared to 0.09 dpa for Xe^{2+} irradiation. At higher temperatures, the amorphization dose increases rapidly.

Table 1. Ion fluence for amorphization of $\text{Cd}_2\text{Nb}_2\text{O}_7$ pyrochlore.

Ion	Temperature (K)	Fluence $\times 10^{14}$ ions/cm ²
Ne^+ (280 keV)	20	11.1
	100	11.4
	130	12.9
	303	25.5
	403	36.6
Xe^{2+} (1200 keV)	20	0.3
	130	0.3
	303	0.7
	473	0.9
	573	2.0
	623	17.0
	673	44.2

Several models have been developed that relate the amorphization dose to temperature and thereby define the critical temperature and activation energy for recrystallization [8-13]. The lines in Fig. 2 were plotted using a recent amorphization-recrystallization model that assumes that recrystallization is maximized when there is a maximum amount of amorphous-crystalline interface:

$$\frac{df_a}{dt} = P(1 - f_a) - \lambda \lambda_a f_a (1 - f_a) \quad (1)$$

In Eq. 1, f_a is the amorphous fraction, t is time, P is the dose rate (dpa/s), and λ is the rate of epitaxial thermal recrystallization. Equation (1) can be solved for the amorphization dose, D :

$$D_c = \frac{\ln P - \ln \frac{P - \lambda_a f_a}{1 - f_a}}{\frac{-\lambda_a}{P} - 1} \sqrt[3]{C} \quad (2)$$

where C is a scaling parameter that relates the damage production rate to the Kinchin-Pease displacement rate. The thermal term, λ , maximizes for $f_a = 0.5$, when there is the most crystalline-amorphous interface. Unlike a more detailed model currently being developed for the case of direct impact amorphization [14], Eq. 1 does not - strictly speaking - say anything about the mechanism of amorphization, except that that recrystallization is most efficient when $f_a = 0.5$. The recrystallization term can be written as:

$$\lambda = \tau_\lambda \exp \frac{-E_\lambda}{kT} \quad (3)$$

Values for τ_λ and E_λ were varied to obtain the best visual fit to the data in Fig. 2. The critical temperature is then given by:

$$T_c = \frac{-E_\lambda}{k \ln \frac{P}{\tau_\lambda}} \quad (4)$$

The values obtained for τ_λ and E_λ and T_c are given in Table 2.

Table 2. Comparison of activation energies and critical temperatures obtained by solving Equations 3 and 6. The amorphization dose at 0 K (extrapolated) and at room temperature are given in the final two columns.

ion	E_a (eV)		T_c (K)		D_0 (0 K) dpa	D_c (RT) dpa
	Eq. 3	Eq. 6	Eq. 3	Eq. 6		
Ne ⁺	0.04	0.04	580	480	0.28	0.65
Xe ²⁺	0.01	0.08	695	620	0.09	0.22

Ion Irradiation and RBS-Channeling

The results of the RBS channeling measurements are summarized in Fig. 3, which also shows the RBS data for an unimplanted Cd₂Nb₂O₇ (111) surface for purposes of comparison. The channeling spectrum for the unimplanted samples was characterized by

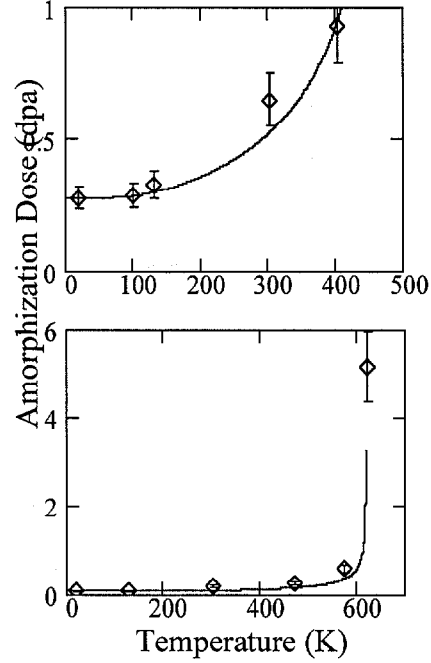


Fig. 2. Amorphization dose as a function of temperature for 280 keV Ne⁺ irradiation (top) and 1200 keV Xe²⁺ irradiation (bottom) of Cd₂Nb₂O₇.

a minimum yield in the range of 3-5%, and the surface peaks for Nb and Cd are clearly distinguishable. With increasing ion dose (Ne^+ or Xe^{2+}), the minimum yield from the channeling spectrum increased relatively rapidly initially and subsequently increased more slowly with increasing ion dose. Finally, at the highest doses, the RBS spectra match the random value in the near-surface region.

Interpretation of the RBS data is difficult because the Cd and Nb damage peaks overlap. As a first approximation, we subtracted the unimplanted spectrum from the implanted spectra in order to remove surface peak contributions. The Cd peak for the intermediate damage spectra became resolvable at channel 900, corresponding to a backscattered He energy of 1975 keV. Using the surface energy

approximation, this corresponds to a depth of 34 nm for the maximum damage peak, compared to 43 nm predicted by SRIM. In order to obtain the disordered fraction on the Cd sublattice, we simply used the ratio I/I_r , obtained from Figure 3. A more accurate analysis would take into account dechanneling effects by using a linear dechanneling approximation [15]. In the present case, because of the shallow depth of the damage peak, the short range of the incident ions, and because of the difficulty in applying the linear dechanneling approximation to these spectra (there is no way to determine where the end of the Cd damage region is actually located), we felt that the best approximation would be obtained by ignoring dechanneling effects. Using these assumptions, the disordered fraction on the Cd sublattice is plotted as a function of dose in Figure 4. Because the slope of the decrease in the Cd yield cannot be accurately determined, however, the Nb data are probably too unreliable for an independent estimation of the disordered fraction. The curves in Fig. 4 were plotted using the well-known Gibbons'

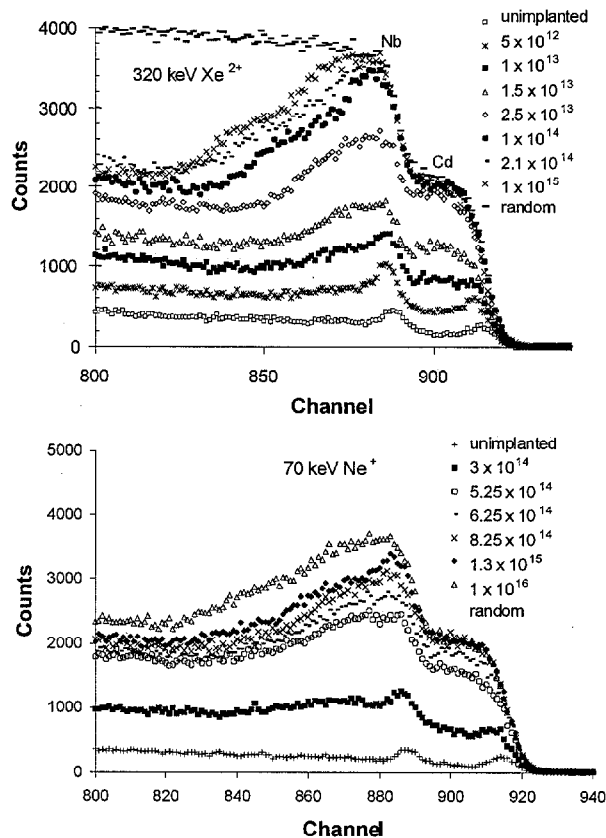


Fig. 3. RBS-Channeling results for $\text{Cd}_2\text{Nb}_2\text{O}_7$.

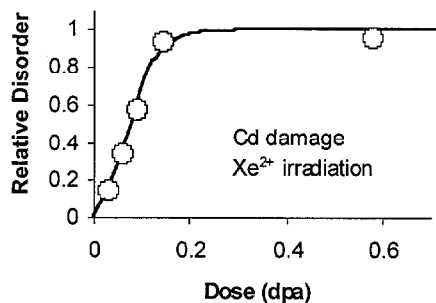


Fig. 4. Relative disorder on the Cd sublattice vs. 320 keV Xe^{2+} ion dose, as obtained from the RBS results. The solid line is Gibbons' "double overlap" model. The results for Ne^+ irradiation were similar.

model [16] for disorder accumulation with increasing dose. For both Ne^+ and Xe^{2+} irradiation, the best-fit curves suggests that amorphization does not occur within individual collision cascades, but may take place more gradually as cascades accumulate and overlap, which is consistent with the electron diffraction results in Fig. 1.

Further Discussion and Conclusion

The results show that $\text{Cd}_2\text{Nb}_2\text{O}_7$ is more susceptible to irradiation-induced amorphization below room temperature than the titanate pyrochlores, but that recovery is more efficient at high temperatures. Sickafus et al. [17] suggested that irradiation-induced amorphization in +3,+4 pyrochlores is controlled by cation radius ratios through their influence on antisite defect formation energies. Accordingly, phases which have radius ratios close to 1:1 have low antisite defect energies and can accommodate radiation damage by cation disordering, without amorphization. $\text{Cd}_2\text{Nb}_2\text{O}_7$ has an A:B cation radius ratio of 1.72:1 (radii from Ref. 18), similar to that of $\text{Gd}_2\text{Ti}_2\text{O}_7$ (1.74:1). Taking either T_c or room-temperature D_c (Table 3) as a measure of the radiation resistance shows that $\text{Gd}_2\text{Ti}_2\text{O}_7$ and $\text{Cd}_2\text{Nb}_2\text{O}_7$ are, however, quite different. If the defect energy picture of amorphization is valid, the relationship between the radius ratios and the antisite defect energies in the +2,+5 pyrochlores must be very different from the +3,+4 phases.

Acknowledgements

The HVEM-Tandem Facility staff assisted with the irradiations. Bill Weber improved the interpretation of the RBS data. AM is supported by NSERC Canada. LAB is supported by the USDOE, Division of Mat. Sci., and RCE by BES/USDOE Grant # DE-FG02-97ER45656. V. Keppens and J. Ramey grew the $\text{Cd}_2\text{Nb}_2\text{O}_7$ crystals. ORNL is managed by the USDOE under contract DE-AC05-00OR22725 (UT-Battelle, LLC).

References

- [1] R.A. McCauley, J. Appl. Phys. **51**, 290 (1980).
- [2] E. Aleshin and R. Roy, J. Am. Ceram. Soc. **45**, 18 (1962).
- [3] S.X. Wang, B.D. Begg, L.M. Wang, R.C. Ewing, W.J. Weber, and K.V.G. Kutty, J. Mater. Res. **14**, 4470 (1999).
- [4] K.L. Smith, N.J. Zaluzec, and G.R. Lumpkin, J. Nucl. Mater. **250**, 36 (1997).
- [5] S.X. Wang, L.M. Wang, R.C. Ewing, G.S. Was, and G.R. Lumpkin, Nucl. Instr. Meth. **B149**, 704 (1999).
- [6] S.X. Wang, L.M. Wang, R.C. Ewing, and K.V.G. Kutty, Nucl. Instr. Meth. **B169**, 135 (2000).
- [7] C.W. Allen and E.A. Ryan, Mat. Res. Soc. Symp. Proc. **439**, 277 (1997).
- [8] K.A. Jackson, J. Mater. Res. **3**, 1218 (1988).
- [9] W.J. Weber, R.C. Ewing, and L.M. Wang, J. Mater. Res. **9**, 688 (1994).
- [10] W.J. Weber, Nucl. Instr. Meth. **166**, 98 (2000).
- [11] G. Carter and M.J. Nobes, J. Mater. Res. **6**, 2103 (1991).
- [12] V. Heera, T. Henkel, R. Kögler, and W. Skorupa, Phys. Rev. B **52**, 15776 (1995).
- [13] S.X. Wang, L.M. Wang, R.C. Ewing, and R.H. Doremus, J. Non-Cryst. Sol. **238**, 198 (1998).
- [14] A. Meldrum, Mat. Res. Soc. Symp. Proc. (these proceedings).
- [15] O.W. Holland, D. Fathy, J. Narayan, and O.S. Oen, Radiat. Eff. **90**, 127 (1985).
- [16] J.F. Gibbons, Proc. IEEE **60**, 1062 (1972).

-
- [17] K.E. Sickafus, L. Minervini, R.W. Grimes, J.A. Valdez, M. Ishimaru, F. Li, K.J. McClellan, and T. Hartmann, *Science* **289**, 748 (2000).
- [18] R.D. Shannon, *Acta Cryst.* **A32**, 751 (1976).